Tripeptides from *Allium subhirsitum* L. extracts: Pharmacokinetics properties, toxicity prediction and *in silico* study against SARS-CoV-2 enzymes and pro-inflammatory proteins

Mejdi Snoussi[1,2*], Emira Noumi[1,3], Amor Mosbah[4], Alaeddine Redissi[4], Mohd Saeed[1], Munazzah Tasleem[5], Mousa Alreshidi[1], Mohd Adnan[1], Ayshah Al-Rashidi[1], Arif Jamel Siddiqui[1], Kaïss Aouadi[6,7], Vincenzo De Feo[8], Adel Kadri[9,10]

[1]Department of Biology, College of Science, University of Hail, Hail, PO Box 2440, Saudi Arabia
[2]Laboratory of Genetics, Biodiversity and Valorization of Bio-resources (LR11ES41), University of Monastir, Higher Institute of Biotechnology of Monastir, Avenue Tahar Haddad, BP74, 5000 Monastir, Tunisia
[3]Laboratory of Bioresources: Integrative Biology and Valorization, (LR14-ES06), University of Monastir, Higher Institute of Biotechnology of Monastir, Avenue Tahar Haddad, BP 74, 5000 Monastir, Tunisia
[4]University of Manouba, ISBST, BVBGR-LR11ES31, Biotechpole Sidi Thabet, 2020 Ariana, Tunisia
[5]School of Electronic Science and Engineering, University of Electronic Science and Technology of China, Chengdu 610054, Sichuan, China
[6]Department of Chemistry, College of Science, Qassim University, Buraidah 51452, Saudi Arabia
[7]University of Monastir, Faculty of Science of Monastir,, Avenue of the Environment, Monastir 5019, Tunisia
[8]Department of Pharmacy, University of Salerno, Via Giovanni Paolo II, 132, Fisciano, Salerno 84084, Italy
[9]Department of Chemistry, Faculty of Science of Sfax, University of Sfax, B.P. 1171, 3000 Sfax, Tunisia
[10]Faculty of Science and Arts in Baljurashi, Albaha University, PO Box 1988, Albaha, Saudi Arabia

Developing new prophylactic and therapeutic agents with broad-spectrum antiviral activities is urgently needed to combat emerging human severe acute respiratory syndrome coronavirus 2 (SARS-CoV-2). Since no available clinically antiviral drugs have been approved to eradicate COVID-19 as of the writing of this report, this study aimed to investigate bioactive short peptides from *Allium subhirsutum* L. (Hairy garlic) extracts identified through HR-LC/MS analysis that could potentially hinder the multiplication cycle of SARS-CoV-2 via molecular docking study. The obtained promising results showed that the peptides (Asn-Asn-Asn) possess the highest binding affinities of -8.4 kcal/mol against S protein, (His-Phe-Gln) of -9.8 kcal/mol and (Gln-His-Phe) of -9.7 kcal/mol towards hACE2, (Thr-Leu-Trp) of -10.3 kcal/mol and (Gln-Phe-Tyr) of -9.8 kcal/mol against furin. Additionally, the identified peptides show strong interactions with the targeted and pro-inflammatory ranging from -8.1 to -10.5 kcal/mol for NF−κB-inducing kinase (NIK), from -8.2 to -10 kcal/mol for phospholipase A2 (PLA2), from -8.0 to -10.7 kcal/mol for interleukin-1 receptor-associated kinase 4 (IRAK-4), and from -8.6 to -11.6 kcal/mol for the cyclooxygenase 2 (COX2) with Gln-Phe-Tyr model seems to be the most prominent. Results from pharmacophore, drug-likeness and ADMET prediction analyses clearly evidenced the usability of the peptides to be developed as an effective drug, beneficial for COVID-19 treatment.

Introduction

The recently declared pandemic coronavirus disease 19 (COVID-19) that causes severe acute respiratory syndrome coronavirus 2 (SARS-CoV-2) is a serious global threat to public health-endangering people's life and floundering in global crisis (1, 2). The recurrent outbreaks induce fatigue, fever, cough, nausea, viral conjunctivitis, loss of smell and taste and severe pneumonia as symptoms resulting in 203 M human infections and 4.3 deaths worldwide in which 532,000 affected cases and 8,311 deaths in the Kingdom Saudi Arabia (KSA), according to the World Health Organization (WHO) as of 10 August 2021 (3, 4). As per the cycle life of coronaviruses, after entering the host cell, the virus replicates via translation of genomic RNA (gRNA), followed by proteolysis of the translated polyprotein with viral 3C-like proteinase and replication of gRNA with the viral replication complex that contains RNA dependent RNA polymerase (RdRp), helicase, 30-to-50 exonuclease, endo RNAse, and 20-O-ribose methyltransferase, and at the end, assembly of all viral

components (5,6). The high spread of the novel coronavirus-related pneumonia COVID-19, as well as its faster ability to transmission from human to human with similar mode as severe acute respiratory syndrome coronavirus (SARS-CoV) and Middle East respiratory syndrome coronavirus (MERS-CoV) (through airborne droplets and contact with infected persons), has motivated research to find new active compounds (7,8).

Due to their large therapeutic effect, and to the lack of specific treatment against SARS-CoV-2, plant-based bioactive molecules remain the best alternative to combat the high spread of this pandemic (9-14). The preferred option is to develop antiviral small molecules to treat infected patients with the convenient bioavailability of commercial drugs. Indeed, short natural bioactive peptides and small molecules have received special attention due to their potential pharmacological properties. In fact, previous studies have reported that small molecules including dipeptides and tripeptides are known to possess several biological activities such as anti-inflammatory, antimicrobial, antiviral, antioxidative stress, anti-apoptosis, opioid, antihypertensive, immunomodulatory and hipoglucemiante properties (15-23). Synthetic dipeptides like Lys-Glu (24), LeuIle (24), and Tyr-Gly (25) are known to possess antitumor activity, neuroprotective effect, and affect the proliferation of peripheral blood lymphocytes, respectively. It was also demonstrated that Kyotorphin (L-tyrosyl-L-arginine), a neuroactive dipeptide, plays a role in pain regulation in the brain (26). The C-capped dipeptides inhibit the RND-family efflux pumps in Gram-negative bacteria (27). The YSV tripeptide, Tyroservatide was described to have antitumor effects on human hepatocellular carcinoma cell line BEL-7402/5-FU (28).

Several small peptide-like proteins are described to possess antiviral activities against a wide range of RNA and DNA virus (29-32). In fact, Carbobenzoxy Di-and Tripeptides were active against Measles virus at levels from 15 to 500 µg/ml (33). Anand and colleagues reported an excellent efficacy of a dipeptide (val-val-acyclovir) against HSV-1 virus using rabbit epithelial and stromal keratitis models. In2012, Panchal and colleagues (34) identified the compound NSC 62914 known to possess antioxidant activity as a molecule with antiviral activity against

the two negative-strand RNA viruses: Ebola viruses (EBOV) and Marburg viruses (MARV). In a literature survey, Agarwal and Gabrani (22), reported the most important antiviral peptides (AVPs) obtained using a computational approach, natural or biological sources. Many authors have designed and simulated peptide-like proteins using computational approaches against SARS-CoV2 structural and accessory proteins (35-37). Using *in silico* approach, Wong and colleagues identified ten peptides from edible insects (VPW, PPY, PIF, VW, PSF, PGF, PAY, VGF, PF and TW) predicted to interact with at least one key binding residue on RBD of spike protein with VPW was the most active among the ten peptides (38). It has been also reported that the S protein-targeting peptides EK1C4, (SARSHRC-PEG4]2- chol, LCB1, and LCB3 show promising antiviral potency against SARS-CoV-2 without affecting the function of the host protein (32). Previous studies have demonstrated that the peptidomimetic furin inhibitor decanoyl-RVKR chloromethylketone (dec-RVKR-cmk) inhibits the activation of different viral glycoproteins (39,40). Using flexible docking and molecular dynamics (MD) simulations, a series of tripeptides were explored as potential neuraminidase (NA) inhibitors and their interactions with the NA protein were then studied (41). Ratho et al. (42) used computational tools to model retrieved sequence of 70 peptides from Antiviral Peptide Database (AVPdb) with receptor-binding domain (RBD) of spike protein and human host receptor ACE2 have shown that peptides have more affinity towards ACE2 in comparison with spike RBD.

Interestingly, it was noticed that most of the peptides bind to RBM (residue binding motif) which is responsible for ACE2 binding at the interface of RBD while, for ACE2, peptides prefer to bind the core cavity rather than the RBD binding interface.

A pharmacophore is a molecular architecture that comprises the crucial characteristics to determine a drug's biological activity. A pharmacophore is a set of steric and electronic properties required for effective supramolecular interactions with a biological target to activate or inhibit its biological response (43). Essential tools for discovering novel hits/leads against any biologically active macromolecule is accomplished through computer-aided drug design tools that include pharmacophore modeling, virtual

screening, molecular docking, and simulation (44). Furin-derived drugs with similar properties against the complex structure (PDB ID: 5MIM) were identified via structure-based pharmacophore modeling. Furin-derived compounds were derived based on the formation of optimum intra-molecular interactions between 5MIM and Furin.

To screen highly diversified small molecules from the Zinc Natural Products database using ZINCPharmer, the Furin-5MIM docked complex was used to generate pharmacophore features (45). Virtual screening approaches are used for drug discovery to discover potential small molecules from a huge database of compounds that interact with the therapeutic target in a time and cost-effective manner (46).

In the present study, we investigated the drug potential of some short natural bioactive peptides from *A. subhirsutum* L. extracts against SARS-CoV-2 coronavirus and pro-inflammatory proteins based on virtual screening, molecular docking, pharmacophore modeling, ADMET and target prediction approaches.

Material and Methods
Plant material sampling and crude extract preparation

The fresh bulbs of *Allium subhirsitum* L. were collected from a local market (Barazan, Hail region, Saudi Arabia) in October 2019. Fresh plant material was dried at room temperature (in shade) and fine powdered, then extracted with methanol and with distilled water (4/40, w/v). The filtrate was concentrated under reduced pressure to yield the crude extract.

Identification of tripeptides by High Resolution-Liquid Chromatography Mass Spectroscopy

Phytochemistry of crude methanolic and aqueous extracts from *A. subhirsutum* L. fresh bulbs were analyzed using UHPLC-PDA-Detector Mass Spectrophotometer (HR-LCMS 1290 Infinity UHPLC System, Agilent 324 Technologies®, USA).

Protein preparation and molecular docking analysis

Different target proteins involved in the different stages of the SARS-Covid-2 life cycle: including binding to lung cells via the ACE2 receptor (PDB ID: 5MIM) and furin protease how to act on S proteins facilitating their interaction with hACE2 receptors (Furin, PDB ID: 5MIM). TMPRSS2 is another serine 2-transmembrane protease that controls the viral entry in the host cell. Structural/accessory and non-structural proteins (NSPs) involved in the synthesis of new viral particles, replication and assembly are also tested including:

☐Receptor Binding Domain of Spike protein known to be exhibited significantly high binding affinity to hACE2 receptor (PDB ID: 6M0J; (47)).

☐Papain-like protease (PLpro) is responsible for the cleavage of polyproteins into 13 non-structural proteins (PDB ID: 6W9C).

☐Chymotrypsin-like protease (3CLpro) is the main protease (Mpro) responsible for the cleavage of polyproteins into non-structural proteins (PDB ID: 6LU7).

☐RNA binding protein (NSP9) involved in both viral genomic RNA reproduction (PDB ID: 6W4B; (48)).

☐ADP ribose phosphatase domain of NSP3 (PDB ID: 6W02) is known to interfere with the host immune response (49).

☐RNA Binding Domain (PDB ID: 6VYO)

☐Endoribonuclease (NSP15, PDB ID: 6VWW) is a hexameric RNA-processing endoribonuclease that preferentially cleaves 3' of uridines.

☐Nucleocapsid protein N-terminal RNA binding domain (PDB ID: 6M3M)

Four pro-inflammatory mediators are also tested including: cyclooxygenase 2 (COX2, PDB ID: 5F1A), phospholipase A2 (PLA2, PDB ID:4UY1), NF−κB-inducing kinase (NIK,PDB ID: 5DN5), and interleukin-1 receptor-associated kinase 4 (IRAK-4, PDB ID: 2NRU).

The three-dimensional (3D) structure of TMPRSS2 protein was prepared using the I-tasser software (50) and the best model with the highest C-score was used. Docking between fifteen receptors and the five peptide-like proteins was carried out by using the AutoDock 1.5.7rc1 software (51). The coordinate of each receptor, free or complexed with inhibitor was extracted from the crystal structure available in the protein data bank (52). During the docking procedure, only amide bonds were defined as rotatable and almost all other bonds were defined as no rotatable. All receptors were kept rigid. Grid maps representing target proteins were constructed with different dimensions depending on the active site of the target

protein (53). The fourteen free 3D molecular structures of the receptors or complexes with inhibitor and the TMPRSS2 were visualized using the molecular visualization software PyMOL (54). The Python Molecular viewer 1.5.6 (55) and the two-dimensional were used to visualize the ligand-protein complex interaction obtained. All two-dimension (D) representations were performed by Discovery Studio Visualizer 20.1.0 software (56).

Molecular target predictions

To estimate the most probable macromolecular targets of a small molecule, assumed as bioactive, the prediction is founded on a combination of 2D and 3D similarity with a library of 370'000 known actives on more than 3000 proteins from three different species by using the web tool (57).

In silico ADME and toxicity profiles

The physicochemical and pharmacokinetics properties of the selected peptides were estimated using ADME (absorption, distribution, metabolism, and excretion) descriptors by a SwissADME online server (http://www.swissadme.ch/). An online ProTox-II webserver (http://tox.charite.de/tox/) was also used to explore the toxicity profiles (hepatotoxicity, immunotoxicity, genetic toxicity endpoints especially cytotoxicity, mutagenicity, and carcinogenicity) of the selected peptides (58-60).

Pharmacophore modeling and virtual screening

Screened molecules from ZINCPharmer were downloaded in SDF format for further analysis. Structure-based virtual screening is applied to identify the best binding conformation of the ligands within the receptor binding site. Compounds obtained through ZINCPharmer were submitted to virtual screening using the GOLD suite to determine the binding affinity and conformation with the receptor structure 5MIM. The resultant binding was analyzed based on the Gold Fitness score to filer the top 100 molecules for pharmacokinetic analysis. Pharmacokinetics and pharmacological properties of top 100 compounds with the highest Gold Fitness Score were identified by 'Calculate Molecular Properties', 'ADMET Descriptor', and 'Toxicity Prediction' protocols from Biovia Discovery Studio v4.5. Furthermore, compound drug safety and efficacy

were evaluated by the 'Filter by Lipinski and Veber Rule' module. The top filtered molecules were docked in the binding pocket of x, y, and z coordinates of 45.527649, -33.178514, and 11.948649, respectively using GOLD Suite. Intra-molecular interactions formed within the docked complex of the top five compounds and 5MIM were evaluated by the 'View Interactions' module from Biovia Discovery Studio v4.5.

Results and Discussion
Tripeptide's structure

Five tripeptides were identified in *A. subhirsitum* extracts (Table 1) with molecular weight ranging from 360.1384 g/mol (Asn-Asn-Asn) to 456.202 g/mol (Gln-Phe-Tyr). No biological activities of these peptide-like proteins were previously described.
Molecular docking

The structures of the five peptides have been the subject of modeling and molecular docking against fifteen "protein" receptors involved in the infection cycle of the CoV-2 virus. The results of binding energies of different receptors (Table 2) revealed a difference in activity or/and in affinity of the different ligands towards the various chosen target proteins and can be classified according to their binding potentials.

The obtained results showed that for the proteins involved in SARS-CoV-2 attachment to host cells (hACE2, furin, TMPRSS2, and S protein) the predicted binding energies were ranging from -8.4 to -9.6 kcal/mol for furin, from -7.2 to -9.8 kcal/mol for hACE2, from -7.4 to -10.3 kcal/mol for TMPRSS2, and from -7.1 to -8.2 kcal/mol for SARS-CoV-2 spike protein. Table 3 shows 2D interaction of top-rate pose from the best two small peptides with hACE2, furin, TMPRSS2, and S protein. The type of binding and the residues involved in the ligand/receptor interaction are also summarized in Table 3.

For the two proteins involved in the cleavage of new synthetized viral proteins into non-structural proteins (M^{pro} and Plp), the predicted energy was ranging from -7.7 to -9.3 kcal/mol for the 3Cl protease, and from -7.4 to -9.1 kcal/mol for Plp. The type of residues/binding implicated in the 2D interaction of the best two small peptides with these two target proteins are listed in table 4
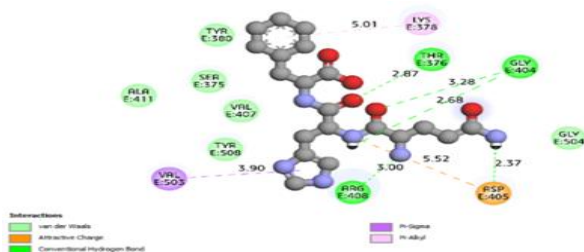
Table 1. List of the five peptide-like proteins identified from *A subhirsitum* L. methanolic and aqueous extracts using HR-LCMS technique

Compound	Retention Time	Molecular Weight	Formula	[*m/z*]	Compound Structure
A. subhirsitum L. methanolic extract					
Asn AsnAsn	0.945	360.1384	$C_{12} H_{20} N_6 O_7$	[*m/z*]* 341.1201	
A. subhirsitum L. aqueous extract					
His Phe Gln	3.988	430.1976	$C_{20} H_{26} N_6 O_5$	[*m/z*]⁻ 411.1797	
Gln His Phe	4.05	430.1978	$C_{20} H_{26} N_6 O_5$	[*m/z*]⁻ 447.1566	
Thr Leu Trp	6.593	418.2222	$C_{21} H_{30} N_4 O_5$	[*m/z*]⁻ 435.1808	
Gln Phe Tyr	7.241	456.202	$C_{23} H_{28} N_4 O_6$	[*m/z*]⁻ 491.1714	

Table 2. Binding affinities of the top-rated pose of the five small peptides-receptor complexes. Binding affinity measured in kcal/mol.

Compounds	SARS-CoV-2 target proteins										
	5MIM	2AJF	TMPRSS2	6M0J	6LU7	6W9C	6W4B	6W02	6VYO	6VWW	6M3M
Asn AsnAsn	-8.4	-7.2	-8.1	-7.1	-7.7	-7.4	-6.1	-7.0	-7.2	-6.8	-6.0
His Phe Gln	-9.2	-9.8	-7.4	-7.2	-8.3	-8.7	-8.0	-7.5	-8.9	-7.4	-7.1
Gln His Phe	-9.3	-9.7	-9.4	-8.2	-8.9	-9.1	-7.4	-8.7	-8.8	-8.8	-7.4
Thr Leu Trp	-9.6	-9.1	-9.8	-7.2	-9.0	-9.2	-7.7	-8.1	-8.6	-7.9	-6.7
Gln Phe Tyr	-9.4	-9.4	-10.3	-8.1	-9.3	-9.0	-7.7	-9.6	-10.2	-8.4	-7.7

Table 3. 2D interaction of top-rated pose of two small peptides-receptor complexes involved in host cell attachment and entry. Binding affinity measured in kcal/mol

2D interactions in the active site and Ligand Receptor Interactions, distance (Å)

Ligand/Receptor Complex: Thr-Leu-Trp/Furin (-9.6 kcal/mol)

van der Waals: Gly265, Pro266, Gly307, Asn310, Tyr313, Asp530, Ala532, Tyr571; **Attractive Charge/Salt Bridge/Pi-Anion:** Glu271 (1.91) (5.19), Trp531 (3.47); **Conventional Hydrogen Bond:** Ser311 (2.47), Gln488 (2.36) (2.52); **Unfavorable Positive-Positive/Donor-Donor:** Ile312(1.21), Arg490 (4.71)

Ligand/Receptor Complex: Gln Phe Tyr/Furin (-9.4 kcal/mol)

van der Waals: Asp154, His194, Val231, Trp254, Asp258, Asp264, Gly265, Pro266, Gly294; **Conventional Hydrogen Bond:** Ser253(2.49), Gly255 (3.36), Asn295 (2.00), Tyr308 (2.26), Ser368 (2.70); **Pi-Anion:** Glu236 (3.90); **Pi-Alkyl:** Leu227 (5.21), Pro256 (5.40)

Ligand/Receptor Complex: His-Phe-Gln/hACE2 (-9.8 kcal/mol)

van der Waals: Phe40, Trp69, Leu73, Thr347, His378, Asp382, Asn394; **Attractive Charge:**Glu375 (4.31); **Conventional Hydrogen Bond:** Ala348 (2.72) (3.30), Asp350 (1.85) (2.33); **Pi-Pi Stacked/Pi-Pi T-shaped:** Trp349 (4.23), Phe390 (4.87)

Ligand/Receptor Complex: Gln-His-Phe/hACE2 (-9.7 kcal/mol)

van der Waals: Phe40, Trp349, Asp350, Asp382, Tyr385, Asn394, His401; **Conventional Hydrogen Bond:** Ser44 (2.59), Ser47 (2.80), Ala348 (2.51); **Carbon Hydrogen Bond:** Ser44 (3.35), Glu402 (3.77); **Pi-Pi Stacked and Pi-Pi T shaped:** His378 (4.62), Phe390 (4.85); **Pi-Alkyl:** Arg393 (4.77)

Ligand/Receptor Complex: Thr-Leu-Trp/Tmprss2 (-9.8 kcal/mol)

van der Waals: Ser111, Cys133, Gly135, Val136, Pro140, Gly141, Gly142, Glu143, Asn146, Arg147, Tyr161, Gln164; **Attractive Charge/Pi-Anion:** His138 (5.10); **Conventional Hydrogen Bond:** Asp134 (2.25), Cys139 (3.37) (3.38), Ser162 (2.47); **Unfavorable Donor-Donor:** Ser162 (2.49); **Pi-Alkyl:** Ile118 (5.39)

Ligand/Receptor Complex: Gln-Phe-Tyr/Tmprss2 (-10.3 kcal/mol)

van der Waals: Ser111, Lys112, Ser130, Gly135, Val136, Ser137, Pro140, Gly 141, Gly142, Cys148, Tyr161, Gln164; **Attractive Charge/Pi-Anion:** His138 (4.07); **Conventional Hydrogen Bond:** Cys133 (1.97), Asp134 (2.99), Cys139 (2.47), Asn146 (2.90); **Carbon Hydrogen Bond:** Ser162 (3.49)

2D interaction in the active site and Ligand Receptor Interactions, distance (Å)	
Ligand/Receptor Complex: Gln-His-Phe/6M0J (-8.2 kcal/mol) **van der Waals:** Ser375, Tyr380, Val407, Ala411, Gly504, Tyr508; **Attractive Charge:** Asp405 (5.52); **Conventional Hydrogen Bond:** Asp405 (2.37), Gly404 (2.68) (3.28), Thr376 (2.87), Arg408 (3.00); **Pi-Sigma:** Val503 (3.90); **Pi-Alkyl:** Lys378 (5.01)	**Ligand/Receptor Complex**: Gln-Phe-Tyr/ 6M0J (-8.1 kcal/mol) **van der Waals:** Leu452, Glu484, Tyr449, Leu492; **Conventional Hydrogen Bond:** Gln493 (2. 28), Ser494 (2.72); **Pi-Pi Stacked:** Phe490 (3.80)
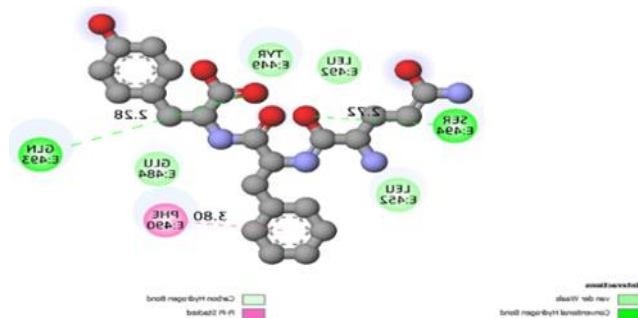
Table 4. 2D interaction of top-rated pose of the best two small peptides with SARS-CoV-2 main protease (M^{pro}, PDB ID: 6LU7) and papain-like protease (PLpro, PDB ID: 6W9C).

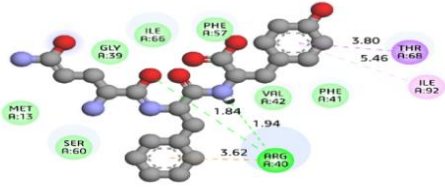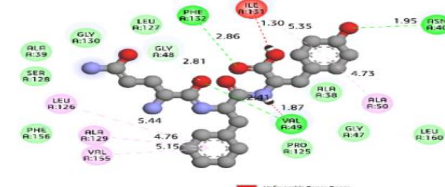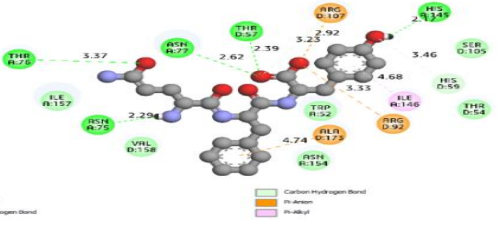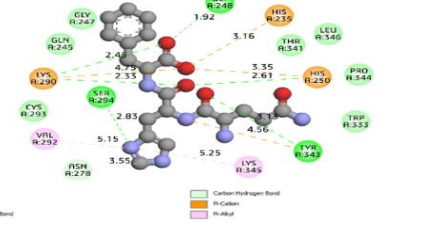| *2D interactions in the active site and Ligand Receptor Interactions, distance (Å)*	
Ligand/Receptor Complex: Thr-Leu-Trp/6LU7 (-9.0 kcal/mol) **van der Waals:** Met49, Phe140, Leu141, Asn142, His163, Leu167, Pro168, Arg188, Gln192; **Conventional Hydrogen Bond:** Ser144 (2.12), Gly143 (2.74), Cys145 (3.67), His164 (3.36), Glu166 (1.86), Gln189 (2.10); **Unfavorable Donor-Donor:** Gly143 (1.84); **Pi-Sulfur:** Met165 (4.46)	**Ligand/Receptor Complex:** Gln-Phe-Tyr/6LU7 (-9.3 kcal/mol) **van der Waals:** Tyr54, Phe140, Leu141, Asn142, Leu167, Pro168, Arg188, Asp187, Thr190; **Conventional Hydrogen Bond:** Glu166 (2.31) (3.91), Gln198 (2.39); **Pi-Cation:** His41 (4.97), Glu166 (4.13); **Pi-Sulfur:** Met165 (5.61); **Pi-Alkyl:** Met49 (4.55)
Ligand/Receptor Complex: Gln-His-Phe/6W9C(-9.1 kcal/mol) **van der Waals:** Thr25, Thr26, Met49, Gly143, Ser144, Met165, His172, Gln189; **Conventional Hydrogen Bond:** Phe140 (2.64), Leu141 (2.23), Asn142 (3.20), Cys145 (2.86) (3.36), His163 (2.52), His164 (2.10), Glu166 (2.55); **Unfavorable Positive-Positive:** His41 (5.23); **Pi-Donor Hydrogen Bond:** Glu166 (3.05)	**Ligand/Receptor Complex**: Gln-Phe-Tyr/6W9C (-9.0 kcal/mol) **van der Waals:** Thr24, Thr25, Cys44, Thr45, Ser46, Tyr54, Cys145, His163, Glu166, Asp187, Arg188, Gln189, Thr190, Gln192, Gly143, Pro168; **Attractive Charge:** His41 (5.55); **Conventional Hydrogen Bond:** Asn142 (2.66) (2.86); **Pi-Alkyl:** Met49 (5.44), Met165 (4.98)
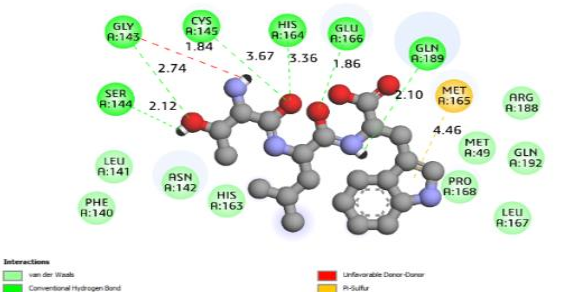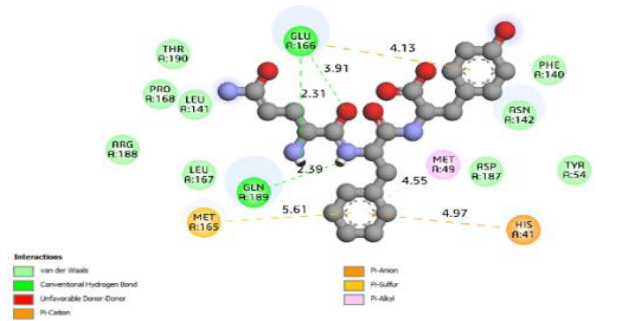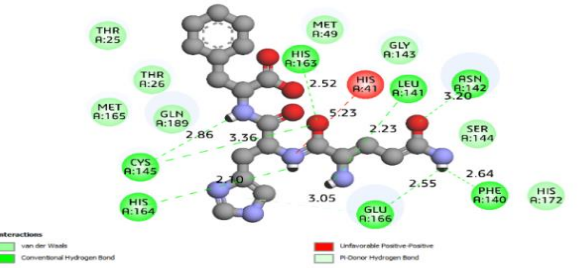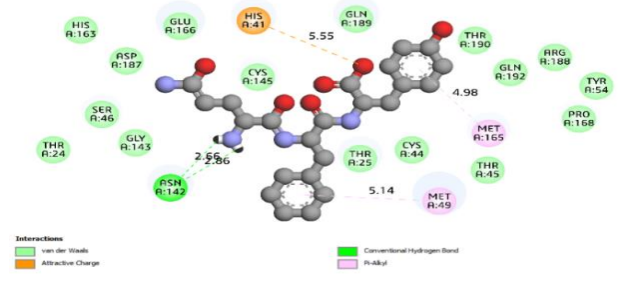
For the proteins involved in SARS-CoV-2 replication/transcription (6W4B, 6WO2, 6VYO, 6VWW, and 6M3M), the results showed also that the highest predicted binding energy was recorded for the tripeptide (Gln Phe Tyr), except the protein (Gln His Phe) with the endoribonuclease (NSP15, PDB ID: 6VWW). The type of residues/binding implicated in the 2D interaction of the best small peptides with these five target proteins are listed in table 5. The five small peptides were also tested against four main targets responsible for SARS-CoV-2 inflammatory reactions. Table 6 shows that the tested molecules were interestingly predicted with high binding energy ranging from -8.1 to -10.5 kcal/mol for NF−κB-inducing kinase (NIK), from -8.2 to -10 kcal/mol for phospholipase A2 (PLA2), from -8.0 to -10.7 kcal/mol for interleukin-1 receptor-associated kinase 4 (IRAK-4), and from -8.6 to -11.6kcal/mol for the cyclooxygenase 2(COX2). The type of the binding and the residues involved in the interaction between (Gln His Phe) and (Gln Phe Tyr) tripeptides with COX2, NIK, IRAK-4, and PLA2 proteins are summarized in Table 7.

Table 5. 2D interaction of top-rated pose of the best small peptides with proteins involved in SARS-CoV-2 replication/transcription

2D interactions in the active site and Ligand Receptor Interactions, distance (Å)

Ligand/Receptor Complex: Gln-Phe-Tyr/6W4B (-7.7 kcal/mol)
van der Waals: Met13, Gly39, Val42, Phe41, Phe57, Ser60, Ile66; **Pi-Cation:** Arg40 (3.62); **Conventional Hydrogen Bond:** Arg40 (1.84) (1.94); **Pi-Sigma:** Thr68 (3.80); **Pi-Alkyl:** Ile92 (5.46)

Ligand/Receptor Complex: Gln-Phe-Tyr/6W02 (-9.6 kcal/mol)
van der Waals: Ala38, Ala39, Gly47, Leu127, Pro125, Ser128, Gly130, Phe156, Leu160; **Conventional Hydrogen Bond:** Asn40 (1.95), Phe132 (2.86), Val49 (2.41); **Carbon Hydrogen Bond:** Gly48 (2.81); **Unfavorable Donor-Donor:** Ile131 (1.30), Val40 (1.87); **Pi-Alkyl:** Ala50 (4.73), Leu126 (5.44), Ala129 (4.76), Val155 (5.15)

Ligand/Receptor Complex: Gln-Phe-Tyr/6VYO (-10.2 kcal/mol)
van der Waals: Thr54, Trp52, Ser105, Asn154, Ile157, Val158,;**Attractive Charge/Pi-Anion:** Arg92 (3.33), Arg105 (2.92), Ala173 (4.74); **Conventional Hydrogen Bond:** Thr57 (2.39), Asn75 (2.29), Thr76 (3.37), Asn77 (2.62), His145 (2.17); **Carbon Hydrogen Bond:** His59 (3.46), Arg107 (3.23).

Ligand/Receptor Complex: Gln-His-Phe/6VWW (-8.8 kcal/mol)
van der Waals: Gln245, Gly247, Cys293, Trp333, Thr341, Pro344, Leu346; **Conventional Hydrogen Bond:** Gly248 (1.92), His250 (2.61), Lys290 (2.33) (2.45), Ser294 (2.83), Tyr343 (3.13); **Carbon Hydrogen Bond:** Asn278 (3.55); **Attractive Charge/Pi-Cation:** His235 (3.16), His250 (3.35), Lys290 (4.75), Tyr343 (4.56); **Pi-Alkyl:** Val292 (5.15), Lys345 (5.25).

Ligand/Receptor Complex: Gln-Phe-Tyr/6M3M (-7.7 kcal/mol).
van der Waals: Gly70, Val73, Ileu75, Asn76, Thr77, Ser79, Gln84, Pro81, Gly138; **Conventional Hydrogen Bond:** Thr136 (2.30), Glu137 (1.93); **Pi-Alkyl:** Pro163 (5.22)
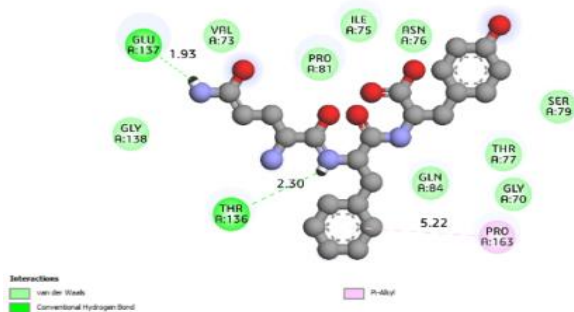

Table 6. Binding affinities of the top-rated pose of the small peptides-receptor complex. Binding affinity measured in kcal/mol

Compounds	Pro-inflammatory mediators			
	4DN5	4UY1	2NRU	5F1A
Asn AsnAsn	-8.1	-8.2	-8.0	-8.6
His Phe Gln	-8.3	-8.5	-10.1	-10.4
Gln His Phe	-10.1	-9.3	-10.1	-11.6
Thr Leu Trp	-8.4	-8.0	-9.5	-10.0
Gln Phe Tyr	-10.5	-10.0	-10.7	-10.9

Taken together, the virtual screening of the five peptide-like proteins with the fifteen target proteins revealed that the Asn-Asn-Asn peptide exhibited the lowest affinity with the different receptors (-6.0 to -8.6 kcal/mol). While the His-Phe-Gln peptide showed two levels of binding energy for two groups of receptors. The first group of complexes detected for 11 receptors with binding energies in the level -7.1 kcal/mol to -8.9 kcal/mol and a second group with strong binding energies between the peptides and the other four receptors (Furin, Tmprss- 2, COX2 and IRAQ) with a binding energy value ranging from -9.2 kcal/mol to -10.4 kcal/mol which are distributed as follows, for His-Phe-Gln/Furin complex (-9.2 kcal/mol), His-Phe-Gln/Tmprss-2 complex (-9.8 kcal/mol), His-Phe-Gln/cox2 (-10.4 kcal/mol) complex and His-Phe-Gln/IRAK complex (-10.1 kcal/mol), respectively.

On the other hand, the two peptides Gln-His-Phe and Thr-Leu-Trp displayed two levels of binding energy, a first level containing complexes with low binding energies ranging from -6.7 to -8.9 kcal/mol and seven complexes ligand-protein with binding energy which in the range -9.1 kcal/mol to -10.1 kcal/mol. It should be noted that the Gln-His-Phe peptide shows a significant affinity for COX2 protein with a binding energy value of -11.6 Kcal/mol.
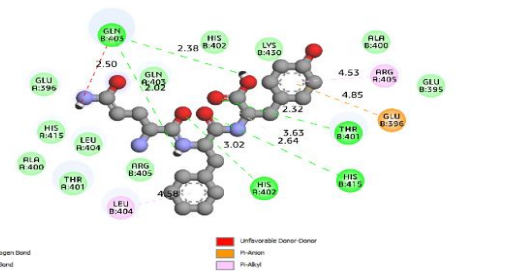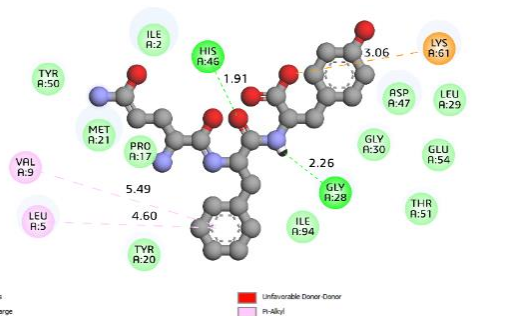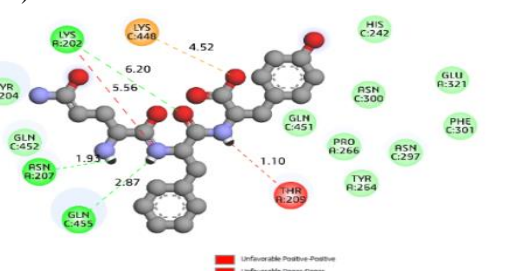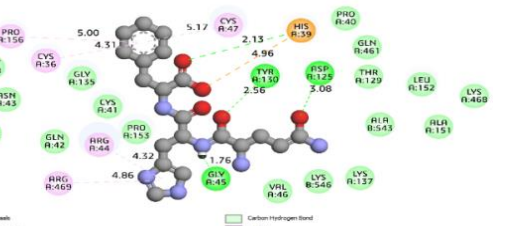
Finally, the Gln-Phe-Tyr model seems to be the most interesting because of its observed high binding energy with the selected receptors. Indeed, this peptide interacts with eleven of the fifteen proteins targeted with binding energies greater than - 9.0 kcal/mol. The other four complexes with binding energies less than -9.0 1 kcal/mol are Gln-Phe-Tyr/RBD, Gln-Phe-Tyr/NSP9, Gln-Phe-Tyr/NSP15 and Gln-Phe-Tyr/RNA binding domain complexes. Interestingly, this peptide had binding energies greater than -10.0 kcal/mol for the pro-inflammatory mediators, Gln-Phe-Tyr/PLA-2 (-10.0 kcal/mol), Gln-Phe-Tyr/NIK (-10.5 kcal/mol), Gln-Phe-Tyr/IRAQ-4 (-10.7 kcal/mol), and Gln-Phe-Tyr/COX2 (-10.9 kcal/mol).

The detailed analysis of the interactions of the different peptide ligands with the receptors allowed us to identify the interaction sites and to detect whether there is interaction with the catalytic triads of the receptors or even the interaction with the activity sites or the metal-binding sites.

For the target protein Furin, the peptides Asn-Asn-Asn, His-Phe-Gln and Thr-Leu-Trp show no interaction with the active site; however, the peptide Gln His Phe binds in the active site of Furin by Ser368 and the metal-binding site with Asp258. The ligand Gln-Phe-Tyr (-9.4 kcal/mol) binds in the active site by interacting with Ser368 and His194 of the catalytic triad and three interactions with the binding site of the Furin substrate, Asp154, Asp264 and Tyr308 and finally one interaction with the metal-binding site, Asp258.

Table 7. 2D interaction of top-rated pose of the best two small peptides four targetable pro-inflammatory mediators.

2D interactions in the active site and Ligand Receptor Interactions, distance (Å)	
Ligand/Receptor Complex: Gln-Phe-Tyr/NIK (-10.5 kcal/mol) **van der Waals:** Glu396, Ala400, Thr401, His402, Gln403, Leu404, Arg405, His415, Lys430, Glu395; **Pi-Anion:** Glu396; **Conventional Hydrogen Bond:** Thr401 (2.32), His402 (3.02), Gln403 (2.02) (2.38), His415 (2.64); **Carbon Hydrogen bond:** His415 (3.63); **Unfavorable Donor-Donor:** Gln403 (2.50); **Pi-Anion**: Glu396 (4.85); **Pi-Alkyl:** Leu404 (4.58), Arg405 (4.53) 	**Ligand/Receptor Complex:** Gln-Phe-Tyr/PLA-2 (-10.0 kcal/mol) **van der Waals:** Ile2, Pro17, Tyr20, Met21, Leu29, Gly30, Asp47, Tyr50, Thr51, Glu54, Ile94; **Attractive Charge:** Lys61 (3.06); **Conventional Hydrogen Bond:** Gly28 (2.26), His46 (1.91); **Pi-Alkyl:** Leu5 (4.60), Val9 (5.49)
Ligand/Receptor Complex: Gln-Phe-Tyr/IRAK-4 (-10.7 kcal/mol) **van der Waals:** Tyr204, Thr208, His242, Tyr264, Pro266, Asn297, Asn300, Phe301, Glu321, Gln451, Gln452; **Attractive Charge:** Lys448 (4.52); **Conventional Hydrogen Bond:** Lys202 (6.20), Asn207 (1.93), Gln455 (2.87); **Unfavorable Positive-Positive/Donor-Donor:** Lys202 (5.56), Tyr209 (1.10) 	**Ligand/Receptor Complex**: Gln-His-Phe/COX2 (-11.6 kcal/mol) **van der Waals:** Asn34, Pro40, Cys41, Gln42, Asn43, Val46, Met48, Thr129, Gly135, Ala151, Leu152, Pro153, Lys468, Gln461, Ala543, Lys137, Lys546; **Attractive Charge:** His39 (4.96); **Conventional Hydrogen Bond:** His39 (2.13), Gly45 (1.76), Asp125 (3.08), Tyr130 (2.56); **Carbon Hydrogen Bond:**……….; **Pi-Alkyl:** Cys36 (4.31), Arg44 (4.32), Cys47 (5.17), Pro156 (5.00), Arg469 (4.86)

For the ACE2 protein, only the peptides Asn-Asn-Asn, His-Phe-Gln and Gln-Phe-Tyr having weaker binding affinity of 7.2 kcal/mol, 9.8 kcal/mol and 9.4 kcal/mol, respectively, blocks the active site by interacting through Glu375. Unlikely, the peptide Gln-Phe-Tyr with the binding energy of -9.4 kcal/mol, interacted with the metal-binding site His378 and Glu402 while the peptides Asn-Asn-Asn, His-Phe-Gln which had binding energy of -7.2 kcal/mol and -9.8 kcal/mol, respectively, only blocks His378. All these results consolidate the suggestion that only the Gln-Phe-Tyr peptide has the potential to block the activity of Furin.

In parallel, it has been shown by Gupta et al. (61) that there is a hot spot on the surface of the protein which is electrostatically favorable for the binding of viral RNA, a positive rich in Arg residues (Arg92, Arg107, Arg149) which directly interact with the RNA of SARS-CoV-2. The analyzes of our results show that the five targeted peptides have an affinity for the RNA binding region (as described above) and block the amino acids Arg92 and Arg107 capable to have an important role in the RNA-protein interaction. The five obtained complexes are Asn-Asn-Asn/RNA binding domain (-7.2 kcal/mol), His-Phe-Gln/RNA binding domain (-8.9 kcal/mol), Gln-His-Phe/RNA binding domain (-8.8 kcal/mol), Thr-Leu-Trp/RNA binding domain (-8.6 kcal/mol) and Gln Phe Tyr/RNA binding domain (-10.2 kcal/mol). These results suggest that Gln-Phe-Tyr may have a strong potential to inhibit RNA/viral protein interaction and maybe a

potential candidate for the treatment of SARS-COVID-19.

Recently, many scientific works have discussed the use of small peptides as an antiviral therapy against COVID19 using computational approaches (62-65). In fact, lactoferrin from breast milk was reported to have antiviral activity against SARS-CoV infection via direct binding to the viral particles or indirectly with host cell receptor or co-receptors (66,67). It has been also demonstrated that peptides retrieved from the Antiviral Peptides Database (AVPdb; (68)) can interact with several target proteins involved in the SARS-CoV2 virus life cycle like the receptor-binding domain of spike protein and hACE2 receptor (42). Interestingly, two peptides namely Sar9 Met (O2)11-Substance P and Sar9 Met (O2)11-Substance P were able to bind to the hACE2 receptor which modulate the interaction of viral particles with its host cell receptors (47).

Molecular and pharmacokinetic properties of the tested tripeptides

To be effective as a drug, the most potent peptides showing the highest binding affinity with the most receptors have been screened for their in-silico drug-likeness and pharmacokinetics to predict their ADME parameters (for Absorption, Distribution, Metabolism and Excretion). Accordingly, the results depicted in Table 8 showed that Thr-Leu-Trp and Gln-Phe-Tyr obeyed Lipinski's rule of five with lower gastrointestinal (GI) absorption following an oral administration. Their predicted lipophilicity given by a consensus log Po/w as the arithmetic mean of the predicted values revealed that they have good permeability and oral absorption through the cell membrane. They also displayed negative skin permeability values with log Kp (SP) = -9.99 cm/s and-11.66 cm/s for Thr-Leu-Trp and Gln-Phe-Tyr, respectively suggesting their little chance to cross the skin. The bioavailability score distinguishes compounds that are poorly permeable from those that are permeable in Caco-2 cells and was found to be 0.55 for two peptides as the same as the known for standard values. Both peptides are predicted to be substrates for P-gp, another pharmacokinetics-relevant protein that serve to protect the central nervous system (CNS) from xenobiotics and they are not able to inhibit any of the cytochromes P450 (CYP1A2,

CYP2C19, CYP2C9, CYP2D6, CYP3A4) involved in the metabolism of xenobiotics, meaning that they have no toxic effect and no accumulation of drug/metabolites.

Prediction of effective drug targets against the top 15% similarity between the five tested tripeptides identified in A. subhirsutum L. extracts (Table 10) revealed some other similar drugs that may be potential against SARS CoV2 (Table 10, Figure 1). Based on the results of toxicity profile, it can be seen (Table 9) that both peptides exhibited comparable toxicity values and are predicted to have no toxic risk against hepatotoxicity, immunotoxicity, carcinogenicity, cytotoxicity, and mutagenicity tests. Maximum targets belong to protease for Asn-Asn-Asn (33.3%), His-Phe-Gln (60%) and Gln-His-Phe (44%), and family AG protein-coupled receptor for Thr-Leu-Trp (56%) and Gln-Phe-Tyr (44%) class.

Many other target classes include enzyme transcription factor, kinase, surface antigen, unclassified protein, lyase, isomerase, ligase, oxidoreductase, and membrane receptor were found, especially for Asn-Asn-Asn and partially for the other peptides (Figure 1).

Pharmacophore modeling and virtual screening

Structure-based virtual screening performed with selected pharmacophore features comprising of 3-hydrogen bond donor and 1-hydrogen bond acceptor (Figure 2) of furin produced 682 molecules from the ZINC Natural Product database. The GOLD suite was employed for executing virtual screening on the compounds within the specified binding pocket of the 5MIM structure to obtain various conformations. Gold Fitness Score for the best conformation of each ligand ranges from 38.03 to 96.43. The top 100 compounds were filtered based on the highest Gold Fitness Score for pharmacokinetic and drug-likeness analysis (69-71). The ADME parameters were evaluated for the top 100 docked compounds, 16 compounds passed Lipinski's rule of five and Veber's rule for oral bioavailability, as shown in Table 11. The physicochemical properties and the toxic profiles of the selected 100 compounds are listed as supplementary materials S1 and S2. These compounds were evaluated for ADME properties using the 'ADMET Descriptor' module from Biovia Discovery Studio.

Table 8. Physicochemical and pharmacokinetic properties of the selected peptides

Small peptides analyzed	Thr-Leu-Trp	Gln-Phe-Tyr
Physicochemical Properties		
Molecular weight (g/mol)	418.49	456.49
Number of heavy atoms	30	33
Number of aromatic heavy atoms	9	12
Number of rotatable bonds	12	14
Number of H-bond acceptors	6	7
Number of H-bond donors	6	6
Molar Refractivity	112.59	119.38
TPSA $Å^2$	157.54	184.84
Consensus log $P_{o/w}$	0.35	-0.29
Lipinski's Rule	Yes	Yes
Pharmacokinetics		
GI absorption	Low	Low
BBB permeant	No	No
P-gp substrate	Yes	Yes
CYP1A2 inhibitor	No	No
CYP2C19 inhibitor	No	No
CYP2C9 inhibitor	No	No
CYP2D6 inhibitor	No	No
CYP3A4 inhibitor	No	No
Log Kp (SP) (cm/s)	-9.99	-11.66
Synthetic accessibility	4.03	3.78
Bioavailability Score	0.55	0.55

Table 9. Prediction of organ, immunotoxicity and genetic toxicity end points of major peptides

	Thr-Leu-Trp		Gln-Phe-Tyr	
	Prediction	Probability	Prediction	Probability
Hepatotoxicity	-	0.69	-	0.71
Immunotoxicity	-	0.70	-	0.73
Carcinogenicity	-	0.99	-	0.99
Cytotoxicity	-	0.82	-	0.78
Mutagenicity	-	0.69	-	0.71

-: inactive

Several compounds were shown to possess good human intestinal absorption level 0 as well as good aqueous solubility at level 3. Cytochrome P450 2D6 (CYP2D6) enzyme inhibition of most of the compounds was observed to be false. However, few compounds show no hepatotoxicity.

The ADMET properties of most of the compounds were within the acceptable range, as shown in Table S1. TOPKAT software from Biovia Discovery Studio was employed for determining the toxicity profile of the compounds.

Table 10. Top 15% macromolecules target similar to the small peptide-like proteins identified in *A. subhirsitum* methanolic and aqueous extracts

Macromolecule's target	Tripeptides identified in *A. subhirsutum* L. extracts				
	Asn-Asn-Asn	His-Phe-Gln	Gln-His-Phe	Thr-Leu-Trp	Gln-Phe-Tyr
Enzyme	13.3	13.3	12	6.7	-
Transcription factor	6.7	-	-	-	-
Kinase	6.7	-	-	-	13.3
Surface antigen	13.3	6.7	-	-	-
Unclassified protein	13.3	-	-	-	-
Lyase	6.7	-	-	-	-
Protease	33.3	60	44	26.7	6.7
Membrane receptor	6.7	-	-	-	13.3
Family AG protein coupled receptor	-	20	36	53.3	40
Isomerase	-	-	4	6.7	-
Ligase	-	-	4	-	-
Reader	-	-	-	6.7	-
Oxidoreductase	-	-	-	-	13.3
Other cytosolic proteins	-	-	-	6.7	-
Other's ion channel	-	-	-	-	6.7

Table 11. Drug-likeness for compounds filtered using Lipinski and Veber Rule Methods from Discovery Studio.

Compounds	TPSA (<140 A$^{\circ 2}$)	MW (< 500)	ALog P (≤ 5)	H-bond donor (≤ 5)	H-bond acceptor (≤ 10)	Rule of 5 violations
ZINC03871579	163.15	230.11	-4.679	4	8	1
ZINC12405062	151.75	286.409	-0.276	5	5	1
ZINC12405060	151.75	286.409	-0.276	5	5	1
ZINC12405061	151.75	286.409	-0.276	5	5	1
ZINC12405063	151.75	286.409	-0.276	5	5	1
ZINC19312827	125.9	331.385	-3.427	6	8	0
ZINC19312821	125.9	331.385	-3.427	6	8	0
ZINC19331307	129.06	333.401	-3.814	7	8	0
ZINC19331315	129.06	333.401	-3.814	7	8	0
ZINC31169859	118.22	344.358	3.025	5	6	0
ZINC31169862	118.22	346.374	2.914	5	6	0
ZINC19331406	125.9	359.438	-2.515	6	8	0
ZINC13377887	107.22	360.401	3.457	4	6	0
ZINC72332946	108.83	427.513	-1.239	6	7	0
ZINC72332945	108.83	427.513	-1.239	6	7	0
ZINC31168041	116.45	432.507	3.725	4	7	0

Abbreviations: TPSA, topological polar surface area; MW, molecular weight; LogP = octanol/water partition coefficient.

The top 100 compounds were tested for toxicity and discovered with no carcinogenic potential, teratogenicity, eye sensitivity or skin rashes; nevertheless, several compounds were found to have developmental toxicity, and low to significant skin and ocular irritation, as presented in supplementary material S2. These compounds were then sorted based on Gold Fitness Score derived from the virtual screening to select the top five compounds for docking and intra-molecular interaction studies. The compounds - ZINC31169862, ZINC19331406, ZINC19331315, ZINC31168041, and ZINC19331307 were found to possess the highest Gold Fitness score of 80.36, 79.04, 78.2, 77.12, and 75.97, respectively,

were further studies for the formation of close in-tra-molecular interactions.
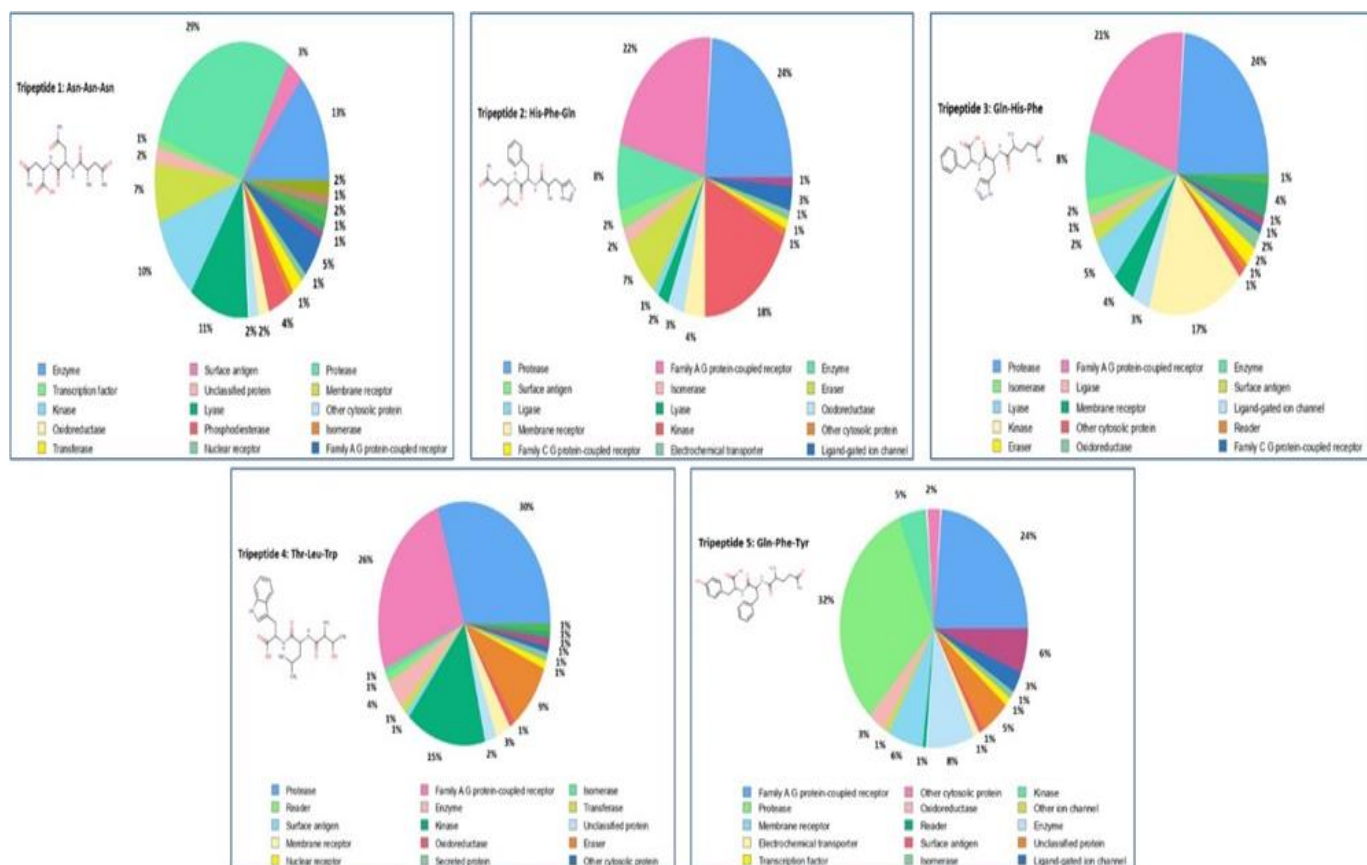

Figure 1. Prediction of drug targets for the identified peptides

All the compounds were observed to form H-bonds with Gln488 and Lys449. Lys449 an active site residue that lies within the conserved domain "P-proprotein", which starts from residue 377 and ends at 463. H-bond formation with an active site residue indicates the formation of a stable complex. Close intra-molecular inter-actions are shown in Table 12 and Figure 3.
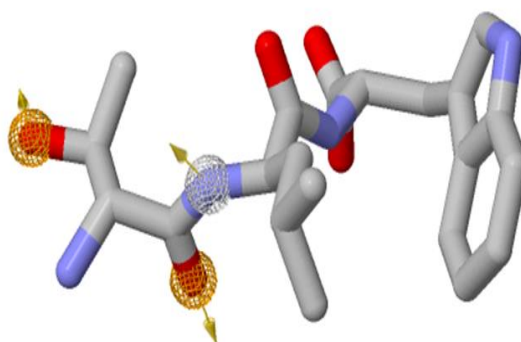

Figure 2. Pharmacophore features generated for Furin on ZINCPharmer. The hydrogen bond donor, and hydrogen bond acceptors features are displayed in mashed spheres of white, and orange, respectively. The orange arrows indicate the constraint direction

Table 12. Top five molecules and their hydrogen bond interactions within the active site of 5MIM

| Compound	Hydrogen Bonds	Gold Fitness Score
ZINC31169862	Ile312, Lys449, Gln488, Ala532, Trp531	80.36
ZINC19331406	Ile312, Lys449, Gln488, Arg490, Tyr571, Ser311	79.04
ZINC19331315	Asn310, Ile312, Lys449, Gln488, Arg490, Tyr571, Gly307, Ser311.	78.2
ZINC31168041	Gly265, Lys449, Gly488, Arg490, Ala52, Tyr571, Gly265.	77.12
ZINC19331307	Asn310, Ile312, Lys449, Gln488, Tyr571, Gly307, Ser311.	75.97
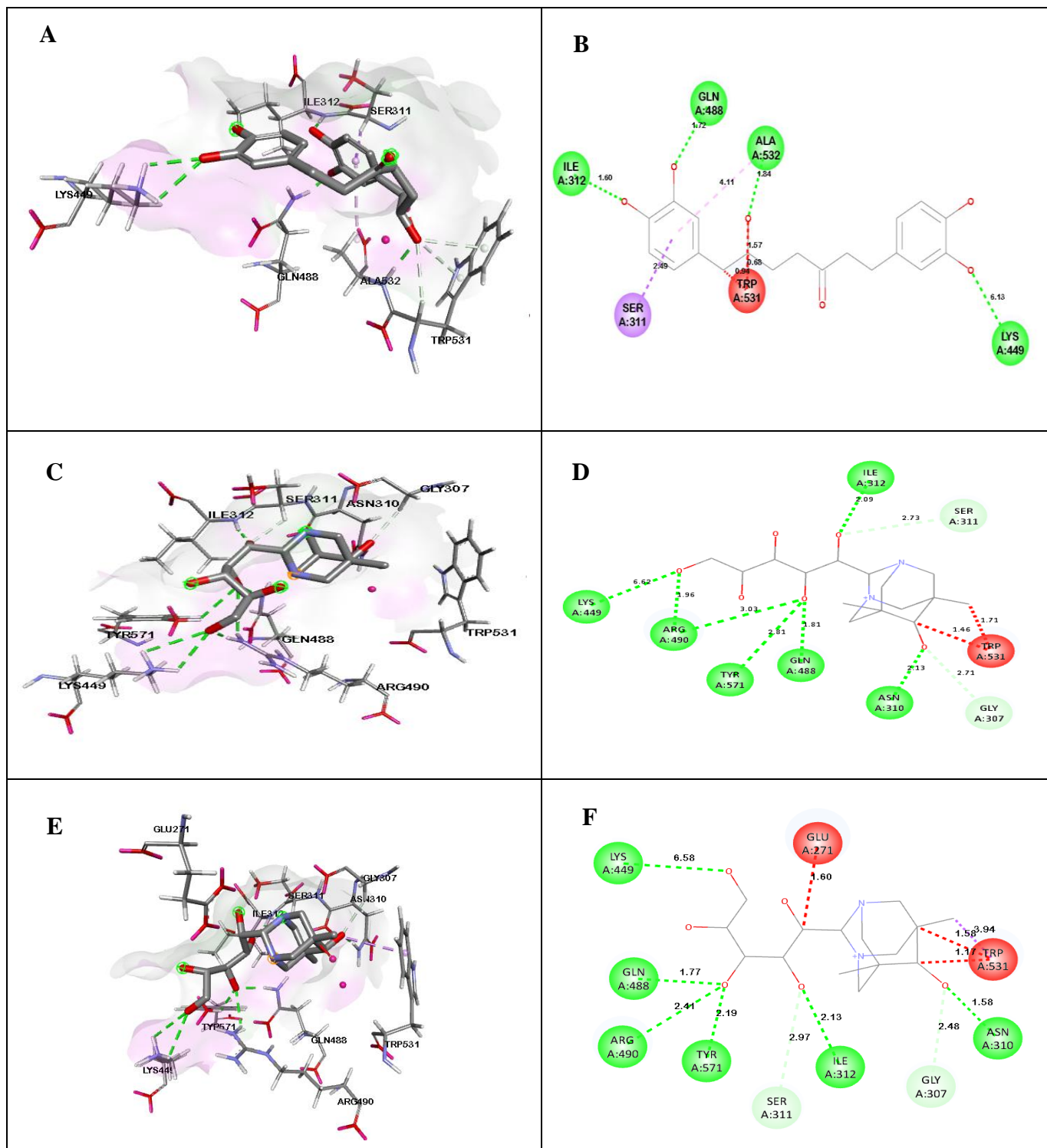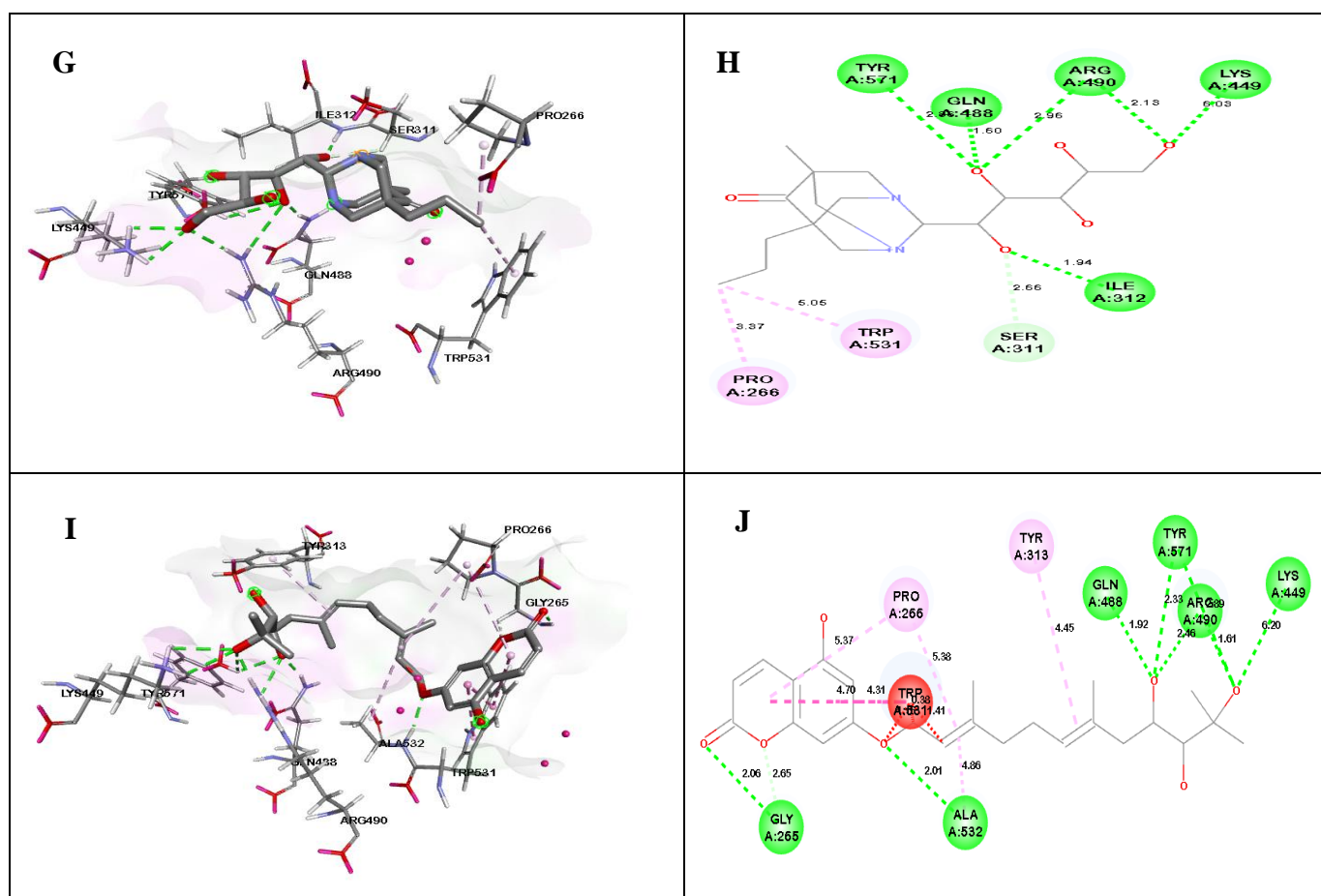
Figure 3. Close intramolecular interactions formed between compounds and 5MIM are shown in 3D and 2D view as visualized in Discovery Studio Visualizer. Green dotted line represents H-bond, sky blue dotted line shows carbon H-bonds and Pi-Donor H-bonds, and purple dotted line describes the hydrophobic interactions. (A) & (B) ZINC31169862 3D & 2D view, (C) & (D) ZINC19331307 3D & 2D view, (E) & (F) ZINC19331315 3D & 2D view, (G) & (H) ZINC19331406 3D & 2D view, and (I) & (J) ZINC31168041 3D & 2D view

Conclusions

The present study was carried to recognize the therapeutic effect of plant-based compounds against the deadly SARS-CoV-2 virus. The results indicate that it may be possible for the five identified tripeptides from A. subhirsutum L. extracts to be potential lead molecules to fight SARS-CoV-2 infection. Interestingly, the structure-based drug design led to the identification of the few most potent compounds; ZINC31169862, ZINC19331406, ZINC19331315, ZINC31168041, and ZINC19331307 that can form H-bonds with the conserved active site residue Lys449 to make a stable complex. However, it is essential to conduct in vitro and in vivo experiments to validate their potency in inhibiting the COVID-19 pandemic.

Funding

Conflicts of Interest

The authors declare no conflict of interest.

References

1. Alam MA, Parra-Saldivar R, Bilal M, Afroze CA, Ahmed MN, Iqbal HMN, Xu J. Algae-Derived Bioactive Molecules for the Potential Treatment of SARS-CoV-2. Molecules 2021, 26(8): 2134.

2. Muchtaridi M, Fauzi M, Ikram NKK, Gazzali MA, Wahab HA. Natural Flavonoids as Potential Angiotensin-Converting Enzyme 2 Inhibitors for Anti-SARS-CoV-2. Molecules 2020, 25(17): 3980. doi:10.3390/molecules25173980

3. Baj J, Karakuła-Juchnowicz H, Teresiński G, Buszewicz G, Ciesielka M, Sitarz EZ, Forma A, Karakuła, K., Flieger, W., Portincasa, P., Maciejewski, R. COVID-19: Specific and Non-Specific Clinical Manifestations and Symptoms: The Current State of Knowledge. Molecules 2020, 9(6): 1753.

4. World Health Organization. Coronavirus Disease 2019 (COVID-19) Situation Report—70. Available online:
https://www.who.int/emergencies/diseases/novel-coronavirus-2019/situation-reports/ (accessed on 2May 2020).

5. Yadav R, Chaudhary JK, Jain N, Chaudhary PK, Khanra S, Dhamija P, Sharma A, Kumar A, Handu S. Role of Structural and Non-Structural Proteins and Therapeutic Targets of SARS-CoV-2 for COVID-19. Cells 2021, 10(4): 821.

6. Anand AV, Balamuralikrishnan B, Kaviya M, Bharathi K, Parithathvi A, Arun M, Senthilkumar N, Velayuthaprabhu S, Saradhadevi M, Al-Dhabi NA, et al. Medicinal Plants, Phytochemicals, and Herbs to Combat Viral Pathogens Including SARS-CoV-2. Molecules 2021, 26(1): 1775.

7. Khan M, Adil SF, Alkhathlan HZ, Tahir M.N, Saif S, Khan M, Khan ST. COVID-19: A Global Challenge with Old History, Epidemiology and Progress So Far. Molecules 2021, 26(1): 39.

8. Mostafa A, Kandeil A, Shehata M, El Shesheny R, Samy AM, Kayali G, Ali MA. Middle East Respiratory Syndrome Coronavirus (MERS-CoV): State of the Science. Microorganisms 2020, 8(7):991.

9. Daoud A, Ben Mefteh F, Mnafgui K, Turki M, Jmal S, Ben Amar R, Ayadi F, ElFeki A, Abid L, Rateb ME, Belbahri L, Kadri A, Gharsallah N. Cardiopreventive effect of ethanolic extract of date palm pollen against isoproterenol induced myocardial infarction in rats through the inhibition of the angiotensin-converting enzyme. Exp. Toxicol. Pathol 2017, 69(8): 656–665.

10. Felhi S, Saoudi M, Daoud A, Hajlaoui H, Ncir M, Chaabane R, El Feki A, Gharsallah N, Kadri A. Investigation of phytochemical contents, *in vitro* antioxidant and antibacterial behavior and *in vivo* anti-inflammatory potential of *Ecballium elaterium* methanol fruits extract. Food Sci. Technol.(Campinas) 2017, 37(4): 558-563.

11. Bakari S, Hajlaoui H, Daoud A, Mighri H, Ross-Garcia JM, Gharsallah N, Kadri A. Phytochemicals. antioxidant and antimicrobial potentials and LC-MS analysis of hydroalcoholic extracts of leaves and flowers of *Erodium glaucophyllum* collected from Tunisian Sahara. Food Sci. Tech. (Campinas) 2018, 38(2): 310-317.

12. Mseddi K, Alimi F, Noumi E, Veettil VN, Deshpande S, Adnan M, Hamdi A, Elkahoui S, Alghamdi A, Kadri A, et al. Thymus musilii Velen. as a promising source of potent bioactive compounds with its pharmacological properties: In vitro and in silico analysis. Arab. J. Chem 2020, 13(8): 6782–6801.

13. Felhi S, Hajlaoui H, Ncir M, Bakari S, Ktari N, Saoudi M, Gharsallah N, Kadri A. Nutritional, phytochemical and antioxidant evaluation and FT-IR analysis of freeze-dried extracts of Ecballium elaterium fruit juice from three localities. Food Sci. Technol 2016, 36(4): 646–655.

14. Alminderej F, Bakari S, Almundarij TI, Snoussi M, Aouadi K, Kadri A. Antioxidant Activities of a New Chemotype of *Piper cubeba* L. Fruit Essential Oil (Methyleugenol/Eugenol): In Silico Molecular Docking and ADMET Studies. Plants 2020,9(11): 1534.

15. Bai F, Town T, Pradhan D, Cox J, Ashish LM, Anderson JF, Flavell RA, Krueger JK, Koski RA, Fikrig E. Antiviral peptides targeting the west nile virus envelope protein. J. Virol 2007, 81(4): 2047-2055.

16. Zhao L, Wang X, Zhang XL, Xie QF. Purification and identification of anti-inflammatory peptides derived from simulated gastrointestinal digests of velvet antler protein (Cervus elaphus Linnaeus). J. Food Drug Anal 2016, 24(2): 376-384.

17. Sánchez A, Vázquez A. Bioactive peptides: A review. Food Qual. Saf. 2017, 1(1): 29–46.

18. Dadar M, Shahali Y, Chakraborty S, Prasad M, Tahoori F, Tiwari R, Dhama K. Antiinflammatory peptides: current knowledge and promising prospects. Inflamm. Res 2019, 68: 125–145.

19. Sangtanoo P, Srimongkol P, Saisavoey T, Reamtong O, Karnchanatat A. Anti-inflammatory action of two novel peptides derived from peanut worms (Sipunculusnudus) in lipopolysaccharide-induced RAW264.7 macrophages. Food Funct 2020, 11: 552–560.

20. Brunetti J, Carnicelli V, Ponzi A, Di Giulio A, Lizzi AR, Cristiano L, Cresti L, Cappello G, Pollini S, Mosconi L, Rossolini GM, Bracci L, Falciani C, Pini A. Antibacterial and Anti-Inflammatory Activity of an Antimicrobial Peptide Synthesized with D Amino Acids. Antibiotics 2020, 9(12): 840.

21. Payoungkiattikun W, Joompang A, Thongchot S, Nowichai B, Jangpromma N, Klaynongsruang S. Evidence of multi-functional peptide activity: potential role of KT2 and RT2 for anti-inflammatory, anti-oxidative stress, and anti-apoptosis properties. Appl. Biol. Chem 2020, 63: 5.

22. Agarwal G, Gabrani R. Antiviral Peptides: Identification and Validation. Int. J. Pept. Res. Ther 2021, 27: 149-168.

23. Saadouli I, Zendah EI, Trabelsi E, Mosbah A, Redissi A, Ferjani R, Fhoula I, Cherif A, Sabatier JM, Sewald N, Ouzari HI. Isolation, Characterization and Chemical Synthesis of Large Spectrum Antimicrobial Cyclic Dipeptide (l-leu-l-pro) from Streptomyces misionensisV16R3Y1 Bacteria Extracts. A Novel 1H NMR Metabolomic Approach. Antibiotics 2020, 9(5): 270.

24. Peters BM, Shirtliff ME, Jabra-Rizk M.A. Antimicrobial Peptides: Primeval Molecules or Future Drugs? PLoS Pathog 2010, 6(10): e1001067.

25. Aluko RE. Technology for the Production and Utilization of Food Protein-Derived Antihypertensive Peptides: A Review. Recent Patents Biotechnol 2007, 1(3): 260–267.

26. Ueda H, Shiomi H, Takagi H. Degradation of kyotoprhin by a purified membrane-bound-aminopeptidase from monkey brain: Potentiation of kyotorphin-induced analgesia by a highly effective inhibitor, bestatin. Life Sci 1985, 36(19): 1865-1871.

27. Okandeji BO, Greenwald DM, Wroten J, Sello JK. Synthesis and evaluation of inhibitors of bacterial drug efflux pumps of the major facilitator superfamily. Bioorg. Med. Chem 2011, 19(24): 7679-89.

28. Shi LX, Ma R, Lu R, Xu Q, Zhu ZF, Wang L, Zhou CL, Li XL, Zhang HL, Yao Z. Reversal effect of tyroservatide (YSV) tripeptide on multi-drug resistance in resistant human hepatocellular carcinoma cell line BEL-7402/5-FU. Cancer Lett. 2008,269(1): 101-110.

29. Elshabrawy HA, Fan J, Haddad CS, Ratia K, Broder CC, Caffrey M, Prabhakar BS. Identification of a broad-spectrum antiviral small molecule against severe acute respiratory syndrome coronavirus and Ebola, Hendra, and Nipah viruses by using a novel high-throughput screening assay. J. Virol 2014, 88(8): 4353-4365.

30. Tamkovich N, Koroleva L, Kovpak M, Goncharova E, Silnikov V, Vlassov V, Zenkova M. Design, RNA cleavage and antiviral activity of new artificial ribonucleases derived from mono-, di- and tripeptides connected by linkers of different hydrophobicity. Bioorg. Med Chem. 2016, 24(6): 1346-1355.

31. Chew MF, Poh KS, Poh CL. Peptides as Therapeutic Agents for Dengue Virus. Int. J. Med. Sci 2017, 14(13): 1342–1359.

32. Schütz D, Ruiz-Blanco YB, Münch J, Kirchhoff F, Sanchez-Garcia E, Müller JA. Peptide and peptide-based inhibitors of SARS-CoV-2 entry. Adv. Drug. Deliv. Rev 2020, 167: 47-65.

33. Miller FA, Dixon GJ, Arnett G, Dice JR, Rightsel WA, Schabel FM, Mclean IW. Antiviral Activity of Carbobenzoxy Di- and Tripeptides on Measles Virus. Appl. Microbiol. 1968 16(10): 1489-1496.

34. Panchal RG, Reid SP, Tran JP, Bergeron AA, Wells J, Kota KP, Aman J, Bavari S. Identification of an antioxidant small-molecule with broad-spectrum antiviral activity. Antiviral Res 2012, 93(1): 23-29.

35. Cannalire R, Stefanelli I, Cerchia C, Beccari AR, Pelliccia S, Summa V. SARS-CoV-2 Entry Inhibitors: Small Molecules and Peptides Targeting Virus or Host Cells. Int. J. Mol. Sci 2020, 21(16): 5707.

36. Han Y, Král P. Computational Design of ACE2-Based Peptide Inhibitors of SARS-CoV-2. ACS nano 2020, 14(4): 5143–5147.

37. Namchuk MN. Early Returns on Small Molecule Therapeutics for SARS-CoV-2. ACS Infect. Dis 2021, 7(6): 1298–1302.

38. Wong FC, Ong JH, Chai TT. Identification of Putative Cell-entry-inhibitory Peptides against SARS-CoV-2 from Edible Insects: An in silico Study. eFood 2020, 1(5): 357-368.

39. Volchkov VE, Feldmann H, Volchkova VA, Klenk HD. Processing of the Ebola virus glycoprotein by the proprotein convertase furin. Proc. Natl. Acad. Sci 1998, 95(10): 5762–5767.

40. Sugrue RJ, Brown C, Brown G, Aitken J, McL Rixon HW. Furin cleavage of the respiratory syncytial virus fusion protein is not a requirement for its transport to the surface of virus-infected cells. J. Gen. Virol 2001, 82(6): 1375–1386.

41. Yang Z, Yang G, Zu Y, Fu Y, Zhou L. Computer-Based *De Novo* Designs of Tripeptides as Novel Neuraminidase Inhibitors. Int. J. Mol. Sci 2010, 11(12): 4932-4951.

42. Rathod SB, Prajapati PB, Punjabi LB. Prajapati KN, Chauhan N, Mansuri MF. Peptide modelling and screening against human ACE2 and spike glycoprotein RBD of SARS-CoV-2. In Silico Pharmacol 2020, 8(1): 3.

43. Qing X, Lee XY, De Raeymaecker J, Tame J, Zhang K, De Maeyer M, Voet A. Pharmacophore modeling: advances, limitations, and current utility in drug discovery. J. Recept. Ligand Channel Res 2014, 7: 81-92.

44. Saeed MSA, Tasleem M, Alabdallah NM, Alam MJ, Asmar ZE, Jamal QMS, Bardakci F, Alqahtani SS, Ansari IA, Badraoui R. Assessment of Antidiabetic Activity of the Shikonin by Allosteric Inhibition of Protein-Tyrosine Phosphatase 1B (PTP1B) Using State of Art: An In Silico and In Vitro Tactics. Molecules 2021, 26(13): 3996.

45. Koes DR, Camacho CJ. ZINCPharmer: pharmacophore search of the ZINC database. Nucleic Acids Res 2012, 40(W1): W409-414.

46. Kumalo HM, Soliman ME. Per-Residue Energy Footprints-Based Pharmacophore Modeling as an Enhanced In Silico Approach in Drug Discovery: A Case Study on the Identification of Novel β-Secretase1 (BACE1) Inhibitors as Anti-Alzheimer Agents. Cell. Mol. Bioeng 2016, 9: 175-189.

47. Egieyeh S, Egieyeh E, Malan S, Christofells A, Fielding B. Computational drug repurposing strategy predicted peptide-based drugs that can potentially inhibit the interaction of SARS-CoV-2 spike protein with its target (humanACE2). PLoS One 2021, 16(1): e0245258.

48. Littler DR, Gully BS, Colson RN, Rossjohn J. Crystal structure of the SARS-CoV-2 non-structural protein 9, Nsp9. BioRxiv 2020, doi: https://doi.org/10.1101/2020.03.28.013920

49. Michalska K, Kim Y, Jedrzejczak R, Maltseva NI, Stols L, Endres M, Joachimiak A. Crystal structures of SARS-CoV-2 ADP-ribose phosphatase:

from the apo form to ligand complexes. IUCrJ . 2020), 7:814-824. https://doi.org/10.1107/S2052252520009653.

50. Yang J, Zhang Y. Protein structure and function prediction using I-TASSER. Curr. Protoc. Bioinformatics 2015, 5.8. 1-5.8. 15. doi.org/10.1002/0471250953.bi0508s52

51. Forli S, Huey R, Pique ME, Sanner MF, Goodsell DS, Olson AJ. Computational protein–ligand docking and virtual drug screening with the AutoDock suite. Nat. Protoc 2016, 11: 905-919.

52. Berman HM, Westbrook J, Feng Z, Gilliland G, Bhat TN, Weissig H, Shindyalov IN, Bourne P.E. RCSB Protein Data Bank: Structural biology views for basic and applied research. Nucleic Acids Res 2000, 28(D1): D235-D242.

53. Snoussi M, Redissi A, Mosbah A, De Feo V, Adnan M, Aouadi K, Alreshidi M, Patel M, Kadri A, Noumi E. Emetine, a potent alkaloid for the treatment of SARS-CoV-2 targeting papain-like protease and non-structural proteins: pharmacokinetics, molecular docking and dynamic studies. J. Biomol. Struct. Dyn. 2021, 13: 1-14. doi: 10.1080/07391102.2021.1946715.

54. Sanner MF. Python: a programming language for software integration and development. J. Mol. Graph. Model 1999, 17: 57-61.

55. Biovia DS. CA, USA: San Diego, 2020. Discovery studio visualizer. 57. http://www.swisstargetprediction.ch/

56. Kadri A, Aouadi K. In vitro antimicrobial and α-glucosidase inhibitory potential of enantiopure cycloalkylglycine derivatives: Insights into their in silico pharmacokinetic, druglikeness, and medicinal chemistry properties. J. Appl. Pharm. Sci 2020, 10(6): 107–115.

57. Othman IMM, Gad-Elkareem MAM, Anouar EH, Aouadi K, Kadri A, Snoussi M. Design, synthesis ADMET and molecular docking of new imidazo[4.5-b]pyridine-5-thione derivatives as potential tyrosyl-tRNA synthetase inhibitors. Bioorg. Chem 2020, 102: 104105.

58. Ghannay S, Kadri A, Aouadi K. Synthesis, in vitro antimicrobial assessment, and computational investigation of pharmacokinetic and bioactivity properties of novel trifluoromethylated compounds using in silico ADME and toxicity prediction tools. Monatsh. Chem 2020, 151: 267–280.

59. Gupta MK, Vemula S, Donde R, Gouda G, Behera L, Vadde R. In-silico approaches to detect inhibitors of the human severe acute respiratory syndrome coronavirus envelope protein ion channel. J.Biomol. Struct.Dyn 2020,39(7): 2617-2627.

60. Elnagdy S, AlKhazindar M. The Potential of Antimicrobial Peptides as an Antiviral Therapy against COVID-19. ACS Pharmacol. Transl. Sci 2020, 3(4): 780−782.

61. Mahendran A, Lim YS, Fang CM, Loh HS, Le C.F. The Potential of Antiviral Peptides as COVID-19 Therapeutics. Front. Pharmacol 2020, 11: 575444.

62. Chowdhury SM, Talukder SA, Khan AM, Afrin N, Ali MA, Islam R, Parves R, Al Mamun A, Sufian MA, Hossain MN, Hossain MA, Halim MA. Antiviral Peptides as Promising Therapeutics against SARS-CoV-2. J. Phys. Chem. B 2020, 124(44): 9785-9792.

63. Khavinson V, Linkova N, Dyatlova A, Kuznik B, Umnov R. Peptides: Prospects for Use in the Treatment of COVID-19. Molecules 2020, 25(19): 4389.

64. Superti F, Ammendolia MG, Valenti P, Seganti L. Antirotaviral activity of milk proteins: lactoferrin prevents rotavirus infection in the enterocyte-like cell line HT-29. Med. Microbiol. Immunol 1997, 186(2-3): 83−91.

65. Ikeda M, Nozaki A, Sugiyama K, Tanaka T, Naganuma A, Tanaka K, Sekihara H, Shimotohno K, Saito M, Kato N. Characterization of antiviral activity of lactoferrin against hepatitis C virus infection in human cultured cells. Virus Res 2000, 66(1): 51− 63.

66. Qureshi A, Thakur N, Tandon H, Kumar M. AVPdb: a database of experimentally validated antiviral peptides targeting medically important viruses. Nucleic Acids Res 2014, 42(D1): D1147–D1153.

67. Bilal I, Xie S, Elburki M, Aziziaram Z, Ahmed S, Jalal Balaky S. Cytotoxic effect of diferuloylmethane, a derivative of turmeric on different human glioblastoma cell lines. Cell Mol Biomed Rep 2021, 1(1): 14-22.

68. Aziziaram, Z., Bilal, I., Zhong, Y., Mahmod, A., Roshandel, M. Protective effects of curcumin against naproxen-induced mitochondrial dysfunction in rat kidney tissue. Cell Mol Biomed Rep 2021,1(1): 23-32.

69. Fujita M, Hirayama T, Ikeda N. Design, synthesis and bioactivities of novel diarylthiophenes: inhibitors of tumor necrosis factor-alpha (TNF-alpha) production. Bioorg. Med. Chem 2002, 10(10): 3113-3122.